RF Performance Measurement of the DSS-14 70-Meter Antenna at C-Band/L-Band

M. S. Gatti
Ground Antenna and Facilities Engineering Section

A. J. Freiley
Radio Frequency and Microwave Subsystems Section

D. Girdner
TDA Mission Support and DSN Operations

The calibration of the 70-meter antenna at C-band (5.01 GHz) and L-band (1.668 GHz) is described. This calibration comes after a modification to an existing L-band feed to include the C-band frequencies. The test technique employs noise-adding radiometers and associated equipment running simultaneously at both frequencies. The test procedure is described including block diagrams, and results are presented for efficiency, system temperature, and pointing.

I. Introduction

For three separate days in October 1988, the RF performance of the 70-meter antenna at DSS-14 was measured. The measurements were done at L-band (1.668 GHz, $\lambda = 17.98$ cm) and C-band (5.01 GHz, $\lambda = 5.98$ cm) to evaluate the efficiency and pointing of the system. The measurements were performed using radiometric techniques with observations of a selected set of celestial radio sources.

The existing L-band feed on DSS-14 [1] has been recently modified to include C-band uplink for support of the Phobos mission. The C-band uplink is designed to handle maximum power of 15 kilowatts, while the L-band channel is receive only. The new C-band feed consists of a disc-on-rod antenna which is located in the center of the existing L-band horn. Future reports will describe the detailed design of the C-band feed [2]. The location of the L/C-band feed on the antenna is such that the phase centers are not located on the focal ring, but are instead located approximately 24 inches from the focal ring. This results in a scanning of the secondary pattern beams from the nominal boresight of the antenna. Both C- and L-band beams are coincident, i.e., they point in the same direction. A significant point of interest is that since the C-band feed is not optimally located, there is a considerable performance degradation from a typical DSN antenna. A preliminary analysis [3] indicated that this configuration will provide satisfactory performance, which the tests described here confirm.

II. Measurement Methodology

The methodology chosen for calibration of the antenna at these frequencies follows closely the techniques used in past programs [4, 5]. Celestial radio sources of known flux densi-

ties, noise-adding radiometers, and azimuth-elevation tracking are used to determine performance. The specific techniques are described below.

A. Radiometric Techniques

The technique used to measure the performance of the antenna was to employ a noise-adding radiometer (NAR) [6], which is standard equipment for calibration of DSN antennas. The system noise power from the feed is combined with modulated noise power from a noise diode, downconverted to an IF signal, and detected with a square-law detector. The square-law detector output is transmitted to the NAR computer and display unit, a BP-80 in this case, which demodulates the signal and calculates Y-factor ratios from which the system noise temperature is computed. In addition, manual Y-factors at the RF frequency were measured and correlated with the NAR with good success. Receiver linearity is always a concern in systems with large dynamic ranges, and was taken into account for these measurements.

B. Measurements

As stated earlier, the objectives of the test were to evaluate the efficiency of the antenna, the system temperature, and pointing at each frequency. These performance measurements of the antenna were made simultaneously at the L- and C-band frequencies.

To measure the efficiency of the antenna, a celestial radio source is acquired and the rise in system noise temperature with respect to the off-source temperature is recorded. The actual measurement sequence consisted of measuring the boresight beam direction, measuring the system temperature when the antenna beam was pointed on source and off source, and performing NAR calibration approximately every hour. This was performed many times during the course of the observation period, i.e., the source was tracked across the sky while continuously moving the beam on and off source. During the course of tracking across the sky, each radio source would move in elevation, first rising, the setting, all the while increasing in azimuth. Therefore, tracking required that the antenna vary in elevation as a function of the time of the track. The result is measurement in efficiency as a function of elevation for each on-off pair. This was performed for several sources, which are listed in Table 1.

The equivalent off-source system temperatures T_{op} as a function of elevation angle are a by-product of the efficiency measurements. The locus of values T_{op} versus elevation (called a tipping curve) are provided, as well as zenith T_{op}.

The antenna was boresighted periodically to update and maintain correct pointing of the antenna beam. A boresight consists of bisecting the beam at the 3-dB points to determine the beam direction. This was done by using a standard strip-chart recorder and commanding the antenna to proceed or follow the source by a fixed angle. The difference in the off-peak levels is balanced manually via appropriate commands to the antenna control system, and the elevation and cross-elevation data is recorded. The offset determined by this measurement is then entered into the antenna pointing system to complete the pointing update.

C. Radio Sources

The sources used for this calibration program included 3C274 (Virgo A), 3C84 (Perseus A), 3C123, 3C295, and 2134+00. The source information and characteristics (flux density, position, etc.) were provided by the Space Physics and Astrophysics Section. Table 1 shows the information assumed for these measurements. The efficiency of the antenna under test is calculated by the ratio of the measured on-off antenna temperature change ΔT_a to the source 100 percent efficiency temperature. The source 100 percent efficiency temperature is related to the flux density of the source S, the physical area of the antenna A_p, and Boltzmann's constant k, and is given by

$$T_s(100\%) = \frac{SA_p}{2k} \tag{1}$$

Note that Table 1 also provides information for source resolution correction C_r. The efficiency therefore is given by

$$\eta = \frac{\Delta T_a}{T_s(100\%)} C_r \tag{2}$$

Of this list of sources, only 3C274 is considered a calibration standard source. This means that the value of $\Delta T_a(100\%)$ in Table 1 for other sources may be significantly in error due to variability; however, these sources are steady enough during the course of a day's observation that relative information may be obtained. Then, by comparing the efficiency for other sources with 3C274 at a common elevation angle, a systematic correction can be determined. At the end of the testing, these corrected source temperatures were provided to the Space Physics and Astrophysics Section as a data point in their database regarding the variability of the source with time. In this way, by observing many sources at different elevation angles, a complete chart of efficiency versus elevation can be generated.

III. Antenna Configuration

A block diagram of the measurement configuration is shown in Fig. 1. A discussion of this configuration follows.

A. Feed/Transmission Lines

The feed is mounted on the side of the XRO feedcone with the waveguides penetrating the cone to connect to the low-noise amplifiers (LNAs). The position of the feed is such that the phase center is located approximately 24 inches outside the focal ring. The L-band waveguide contains an L-band low-pass filter, couplers for signal injection and sampling, and a waveguide switch. The waveguide switch allows either the feed or an ambient load to be connected to either of the two LNAs. The C-band waveguide also contains couplers, a switch and ambient load, and the capability for water cooling.

B. Receiver

The L-band receiver used in these measurements consisted of the L-to-S upconverter and operational Block IV receiver. The IF signal from the receiver was tapped into at the alidade where the NAR instrumentation was located. This allowed for a complete calibration of the L-band system and minimized additional cable runs.

The C-band system normally operates as transmit only, therefore, an R&D receiver was installed temporarily until the operational calibration receiver could be delivered. The receiver used was the same one used to perform calibration tests of the feed at the Microwave Test Facility (MTF) at Goldstone.

C. Other Instruments

Other instruments that completed the measurement system included the noise diodes, located in the cone, a JPL-designed BP-80 NAR, square-law detectors, noise-diode controllers, power meters, filters, and spectrum analyzers. The noise-diode controllers were used both as modulators of the noise-diode sources in the cone, and as on/off switches for the diodes for use in receiver linearity checks. The spectrum analyzer was used to view the receive band of frequencies for RFI, which was at times a serious problem. When RFI was present, appropriate filters at the IF frequency were used.

IV. Test Results

A. Pointing/Subreflector Positioning

The pointing data acquired in these tests not only aided in defining the antenna efficiency, but also provided data to better define the total errors of the 70-meter pointing system. Pointing data from measurements of any feed position also provide information in the ongoing iterative process of blind pointing improvement.

For pointing, a datum must be chosen from which pointing may be referenced. This datum is a model of how the antenna performs given many different input parameters such as gravity, preset elevation and azimuth offsets, etc. For these tests, the datum consisted of a model derived from calibration data taken in mid-August 1988 on the XKR feedcone, referred to here as the XKR model. The pointing model for this feedcone was selected because the pattern of this X-band feed is the narrowest. The location of the L/C-band feed is known with respect to the XKR feedcone; therefore, predictions regarding the beam pointing were made and only those parameters changed in the model. All data were taken from this initial L/C-band pointing model. Offsets in the actual beam pointing from the direction of the model were measured during the course of observations. All offsets measured fell within +5 to −3 millidegrees in elevation and within −2 to −7 millidegrees in azimuth cross-elevation. The small size of these offsets indicates that the initial L/C-band pointing model is fairly accurate.

The original model for the L/C-band antenna was updated as a result of these tests and the elevation and cross-elevation beam pointing directions are shown in Table 2. The pointing directions in Table 2 reflect the latest updates due to this sequence of tests. In this table, column 2 shows the position of the XKR radar beam (the datum), column 3 shows the position of the C-band, and column 4 shows the delta between the XKR and C-band. Columns 5 and 6 are for L-band positions and deltas. The last column shows the pointing difference between the C-band and L-band beams.

B. System Noise Temperature

The intrinsic noise temperature of the antenna at both C-band and L-band was measured using two separate techniques. The first technique consisted of a manual Y-factor measurement of the RF signal using a tuned RF receiver (TRF) which consisted simply of a post-LNA amplifier, bandpass filter, isolator, and power meter. The second technique was to use the NAR instrumentation as discussed above. In both of these techniques, the results agreed to within a few percent. Also, an analysis of the configuration was done to estimate the noise temperature. The actual and predicted values for the zenith T_{op} are given in Table 3. Table 4 gives the various components that make up the predicted values of T_{op}.

In addition, the system temperature as a function of elevation was measured during the course of the efficiency calibration. These data for C-band are given in Fig. 2, and for L-band in Fig. 3. Shown in these figures are the composite data for all days' observations. Also shown on both of these curves are data resulting from tipping the antenna in elevation while measuring the system temperature. This curve is highlighted by the solid line.

C. System Gain/Efficiency

The system gain is calculated by multiplying the efficiency by the maximum theoretical gain which is given by

$$G_{100} = \left(\frac{\pi D}{\lambda}\right)^2 \quad (3)$$

where D = the antenna diameter (70 meters), and λ = the operating wavelength. The measurement of the system efficiency is obtained from Eq. (2) given in Section II. Like the tipping curve, the efficiency is given as a function of elevation, due to the motion of the radio source across the sky. The efficiency versus elevation for C-band is given in Fig. 4, and for L-band in Fig. 5.

D. Receiver Linearity

Linearity may be a problem for receivers that are expected to operate across a large dynamic range. The large dynamic range of the NAR is required because the on-source/off-source signal levels are often quite different. In addition, the calibration of the NAR uses an ambient load which is a factor of 5 to 10 times increase in power over the system noise power. To assure that the receiver is producing the correct results, a technique of systematically adding a small excess noise to the measurement is used. This noise is added to the signal during calibration, when the system temperature is near 350 K, and then during off-source noise measurement, when the system temperature is near 100 K. If the system is linear, the value of excess noise added at each end of the dynamic range will be the same. Any required corrections follow the techniques developed earlier [7] and consist of fitting a second-order equation to the results of four measurements of the following:

(1) Ambient load plus the excess noise

(2) Ambient load

(3) Antenna plus excess noise

(4) Antenna

From the second-order fit, corrections may be applied to subsequent measured data.

V. Conclusions

The 70-meter antenna has been upgraded to include C-band transmit by modifying the existing L-band feed. Calibrations of the C-band and L-band feed were presented including efficiencies, system temperatures, and pointing. It is noted that the antenna beams are offset from the nominal boresight axis due to the lateral displacement of the feed. The antenna efficiency is therefore lower than could be achieved if the subreflector was moved to a more optimum position. This is a possible area of improvement if required in the future. The measurements provided valuable pointing data which may be used as baselines for other pointing calibrations.

References

[1] J. Withington, "DSN 64-Meter Antenna L-Band (1668-MHz) Microwave System Performance Overview," *TDA Progress Report 42-94*, vol. April–June 1988, Jet Propulsion Laboratory, Pasadena, California, pp. 294–300, August 15, 1988.

[2] P. Stanton, "The L/C-Band Feed Design for the DSS-14 70-Meter Antenna (Phobos Mission), in preparation, Jet Propulsion Laboratory, Pasadena, California.

[3] D. Hoppe and P. Stanton, "Calculated 70-Meter Antenna Performance for Offset L-Band and C-Band Feeds," *TDA Progress Report 42-90*, vol. April–June 1987, Jet Propulsion Laboratory, Pasadena, California, pp. 12–20, August 15, 1987.

[4] A. J. Freiley, "Radio Frequency Performance of DSS 14 64-Meter Antenna at X-band Using an Improved Subreflector," *TDA Progress Report 42-60*, vol. September–October 1980, Jet Propulsion Laboratory, Pasadena, California, pp. 168–176, December 15, 1980.

[5] A. J. Freiley, "Radio Frequency Performance of DSS 14 64-m Antenna at X-Band Using a Dual Hybrid Mode Feed," *DSN Progress Report 42-53*, vol. July–August 1979, Jet Propulsion Laboratory, Pasadena, California, pp. 132–139, October 15, 1979.

[6] P. D. Batelaan, R. M. Goldstein, and C. T. Stelzried, "A Noise-Adding Radiometer for Use in the DSN," *JPL Space Programs Summary, 37-65*, vol. II, Jet Propulsion Laboratory, Pasadena, California, pp. 66–69, 1970.

[7] C. T. Stelzried, "Non-Linearity in Measurement Systems: Evaluation Method and Application to Microwave Radiometers," *TDA Progress Report 42-91*, vol. July–September 1987, Jet Propulsion Laboratory, Pasadena, California, pp. 57–66, November 15, 1987.

Table 1. Celestial radio source list for C- and L-band calibrations

Radio source	Position, R.A., 1950 Dec, 1950	L-band			C-band		
		Flux density, jansky	T_s, 100%, kelvin	Source resolution correction, C_r	Flux density, jansky	T_s, 100%, kelvin	Source resolution correction, C_r
3C274	12:28:17.6 +12 40 01.7	183.99	256.44	1.2	71.89	100.2	1.19
3C84	07:16:29.6 +41 19 51.9	52.77	73.542	1.0	48.49	67.584	1.0
3C123	04:33:55.2 29 34 14.0	42.38	59.061	1.001	16.48	22.970	1.0099
3C295	14:09:33.5 +52 26 13	19.19	26.747	1.0	6.36	8.865	1.0
2134+00	21:34:05.1 00 28 27.0	8.28	11.54	1.0	9.18	12.801	1.0

Table 2. Pointing directions of the C- and L-band antenna

Parameter	XKR radar beam position, mdeg	C-band, mdeg	ΔC-band, mdeg	L-band, mdeg	ΔL-band, mdeg	ΔC to L, mdeg
Cross-elevation	−11.5	145.9	134.4	155.6	144.1	+9.7
Elevation	+14.8	−79.7	−64.9	−81.5	−66.7	−1.8

Table 3. Measured and predicted zenith system noise temperatures

Band	Tuned RF receiver, K	Noise-adding radiometer, K	Prediction, K
L-band	35.3	35.7	40
C-band	121	116	124

Table 4. Summary of elements making up the zenith T_{op} prediction

Component	Symbol	L-band value, K	C-band value, K
Feed	T_f	8.15	26.64
Transmission line	$T_{w/g}$	3.75	5.90
Spillover	T_s	7.8	11.1
Quad-leg scattering	T_{qs}	2.6	2.6
LNA temperature	T_m	12.0	71.5
Follow-up amplifier temperature	T_f	1.0	1.0
Atmosphere	T_{atm}	2.0	2.5
Galactic temperature	T_{gal}	2.7	2.7
Total	T_{op}	40.0	123.94

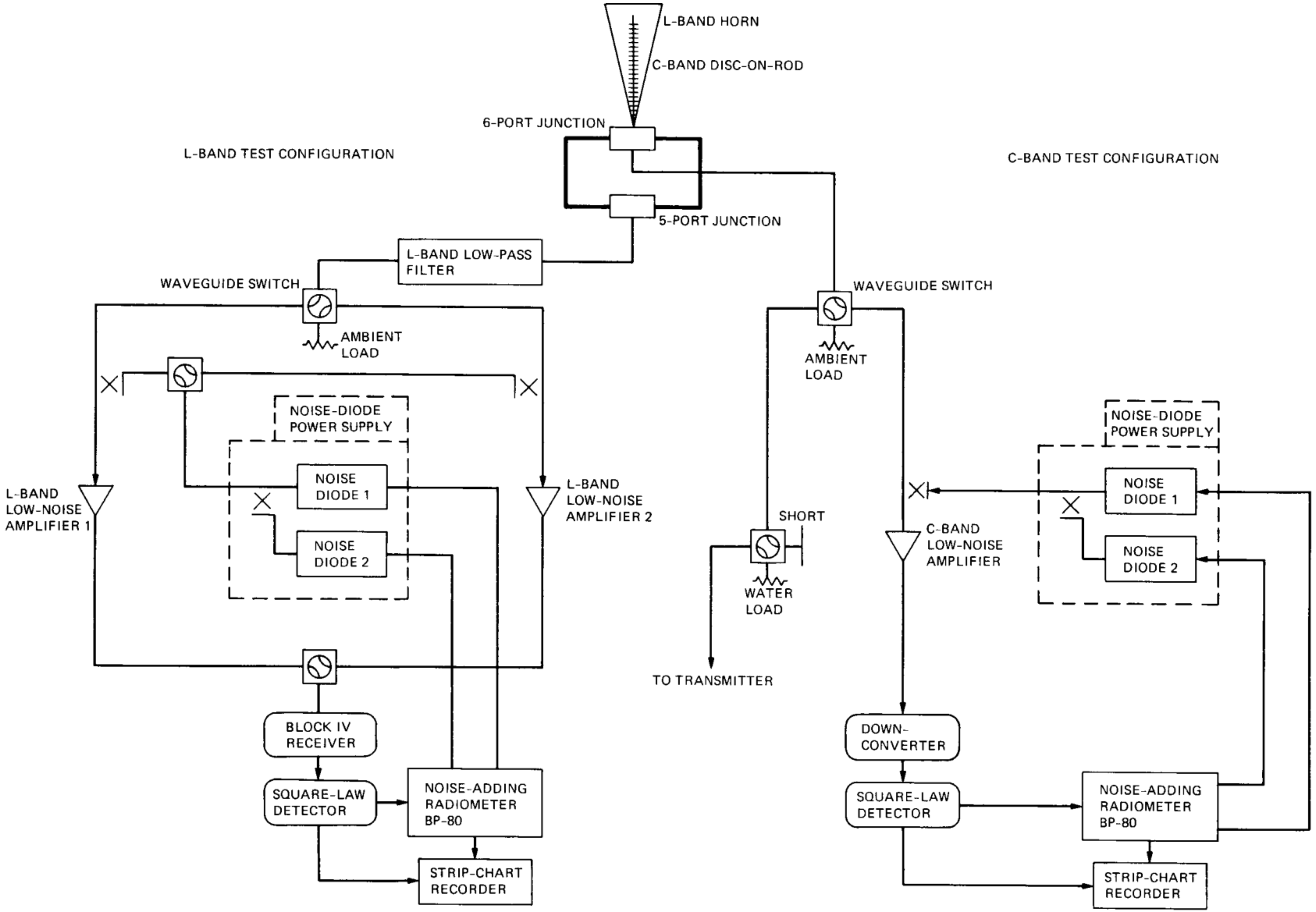

Fig. 1. Block diagram of C/L-band test configuration.

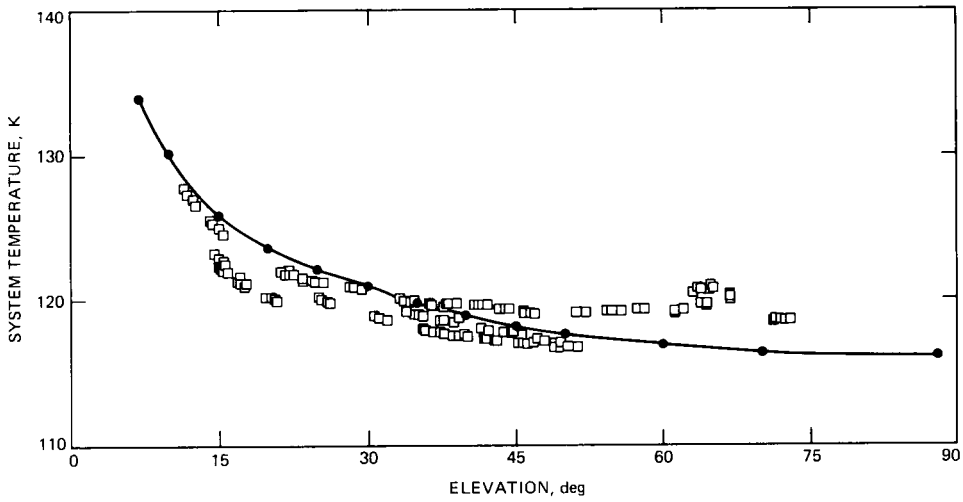

Fig. 2. C-band system temperature.

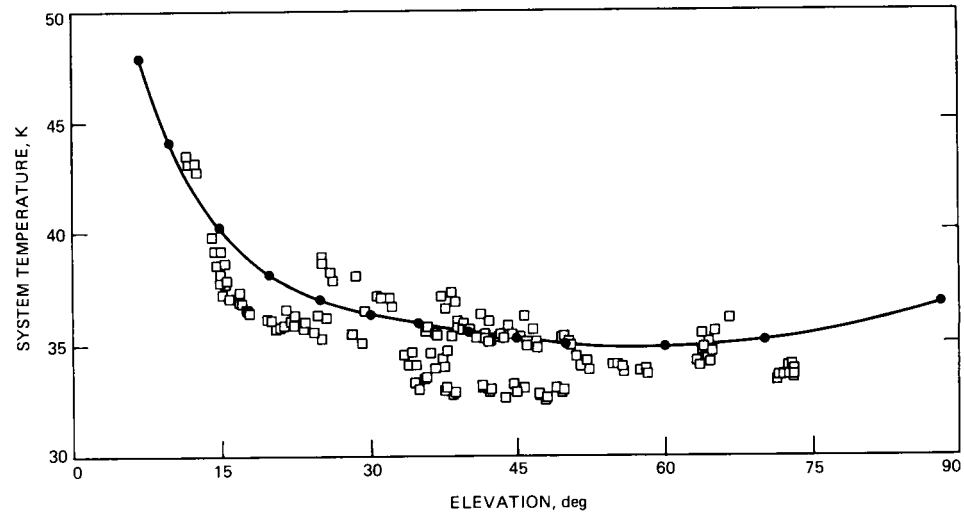

Fig. 3. L-band system temperature.

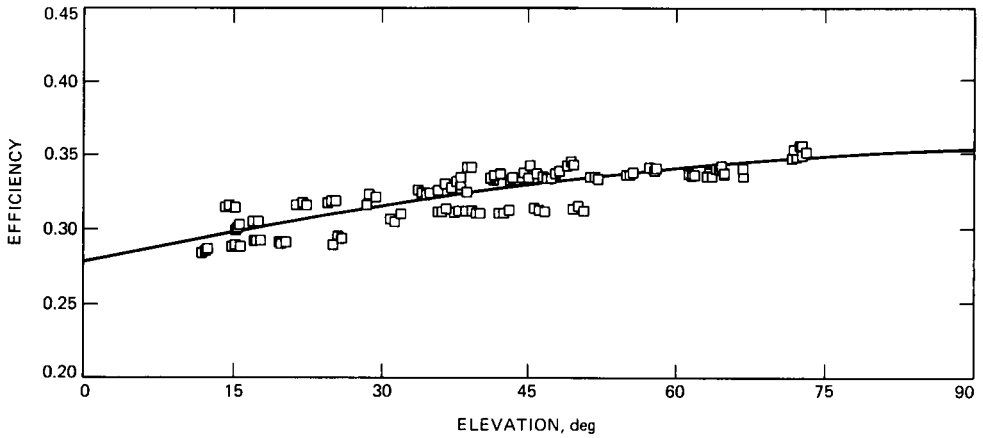

Fig. 4. C-band efficiency versus elevation.

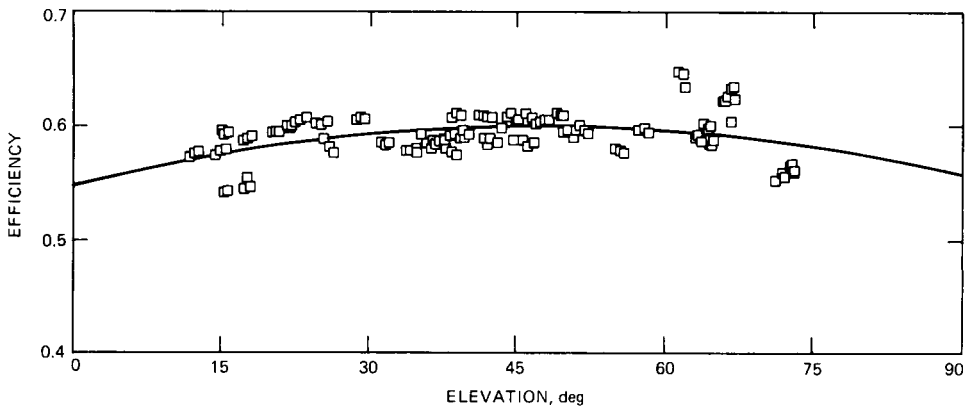

Fig. 5. L-band efficiency versus elevation.